Dynamic Modeling and Simulink Simulation of a Shallot Planter Union

HAU LE T[1], QUANG NGUYENT[2], DANG NGUYENTH[1], PHI CAOH[1,*]
[1]Vinh Long University of Technology Education,
Vinh Long,
VIETNAM

[2]Faculty of Automotive Technology,
Hanoi University of Industry,
Ha Noi,
VIETNAM

*Corresponding Author

Abstract: - This study develops a coupled dynamic model and MATLAB/Simulink simulation framework for a shallot planter union consisting of a tractor, a working machine, a planting head, and an elastic coupling joint operating on soft soil. An eight-degree-of-freedom formulation is established using the Euler–Lagrange method and converted into a state-space representation with 16 state variables and 10 terrain-induced excitation inputs. Soil reaction is described via the Bekker pressure–sinkage relationship and linearized around the operating range for efficient simulation. The eigenvalue analysis confirms asymptotic stability of the coupled system ($\max R(\lambda) = -2.8782$), and time responses under initial perturbations remain bounded. Simulations indicate that pulse-type excitation governs peak responses, particularly in coupling yaw motion and planting head displacement, while harmonic and random excitations mainly contribute to sustained vibration levels. Frequency response analysis shows dominant low-frequency amplification of the main-body vertical motions in the range of approximately 0.5–2 Hz. The proposed framework supports preliminary vibration assessment and parameter tuning of shallot planting machinery under weak-soil field conditions.

Key-Words: - Shallot planter union, tractor-implement dynamics, Euler-Lagrange formulation, state-space modeling; MATLAB/Simulink, Bekker pressure-sinkage, soft-soil interaction, vibration and peak-load assessment.

Received: January 9, 2026. Revised: March 15, 2026. Accepted: April 11, 2026. Published: July 13, 2026.

1 Introduction

Dynamic modeling and vibration analysis of agricultural tractor–implement systems have attracted increasing research interest due to their significant influence on operational stability, soil–tool interaction, and planting performance under real field conditions. Recent advances in digital modeling environments have enabled the construction of nonlinear and multi-degree-of-freedom dynamic models that capture complex interactions among vehicle structures, implements, and terrain. [1] proposed a nonlinear dynamic model for agricultural vehicles constructed in a digital space, demonstrating the potential of integrated virtual modeling for system-level dynamic analysis.

Soil–vehicle interaction remains a major source of excitation in agricultural machinery dynamics. The mechanical properties of soft and deformable soils strongly affect vibration transmission and load transfer, particularly during low-speed field operations. Bekker's classical terrain-vehicle theory [2] continues to provide a widely adopted foundation for modeling soil pressure–sinkage relationships, while more recent studies have quantified soil stiffness parameters using physical soil properties to improve model realism, [3]. Such formulations enable a practical representation of soil compliance while maintaining computational efficiency in dynamic simulations.

Multi-body dynamics approaches have been increasingly applied to agricultural vehicles to capture coupled vertical, rotational, and lateral motions. Tractor dynamics simulations incorporating human–machine interaction [4], articulated steering mechanisms [5], and autonomous control-oriented multibody models [6] have demonstrated that simplified rigid-body formulations may underestimate transient loads and vibration amplitudes. Recent investigations have further expanded multibody modeling toward deformable terrain interaction and simulation-to-reality gap analysis, emphasizing the sensitivity of dynamic responses to contact modeling assumptions and parameter selection, [7], [8].

From a methodological perspective, state-space modeling and dynamic system formulations provide a systematic framework for stability assessment and transient response analysis in multi-degree-of-freedom mechanical systems. [9] presented a dynamic modeling and simulation approach for a multi-degree-of-freedom suspension system, illustrating the application of state-space representations to vibration and stability analysis in complex mechanical assemblies. Although not specific to agricultural machinery, such methodological contributions establish a relevant theoretical basis for the state-space and stability analyses adopted in the present study.

Despite these advances, many existing tractor–implement models primarily focus on the tractor body or lateral dynamics, while the combined effects of coupling joint dynamics, yaw motion, planting unit vibration, and soil–tool interaction are often simplified or treated independently. Recent studies on generalized tractor–trailer systems and stability control, [10], [11], as well as real-time state estimation for agricultural tractors [12], highlight the importance of accurately representing coupling dynamics and system states. However, an integrated dynamic framework that explicitly captures tractor–implement–soil interaction with coupling and planting head dynamics remains limited. This gap motivates the development of the coupled dynamic model proposed in this study.

2 Problem Formulation

2.1 Dynamic Model of the Shallot Planter Union

2.1.1 System Description

The shallot planter union consists of a tractor and a working machine connected via a low rigidity coupling joint, with a shallot planting head in direct contact with the field surface. For dynamic modeling, the distributed masses of the tractor, working machine, and planting head are represented by equivalent lumped masses located at their respective centers of gravity. The planting mechanism places shallot seedlings at the prescribed spacing and depth to ensure favorable growing conditions Figure 1.

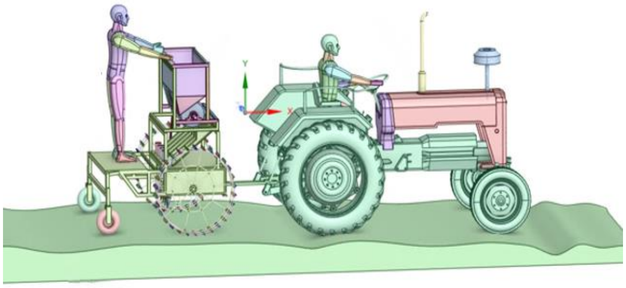

Fig. 1: Schematic illustration of the shallot planter union
Source: created by the authors

2.1.2 Modeling Assumptions

To ensure tractable analytical derivation and efficient numerical simulation, the following assumptions are adopted:

i. The longitudinal motion along the planting bed is steady and forward speed variations are neglected.
ii. Motions consist of small oscillations about the static equilibrium, enabling linearization.
iii. Soil–machine interaction follows the Bekker pressure–sinkage relationship and is linearized within the operating range.
iv. Large slip, lateral skidding, and aerodynamic resistance are neglected due to low operating speed.
v. Components behave like rigid bodies with masses concentrated at their centers of gravity.

Based on these assumptions, the equivalent dynamic model of the coupled tractor–working machine–shallot planting head system, including the generalized coordinates, elastic coupling, and soil–tool interaction, is presented in Figure 2.

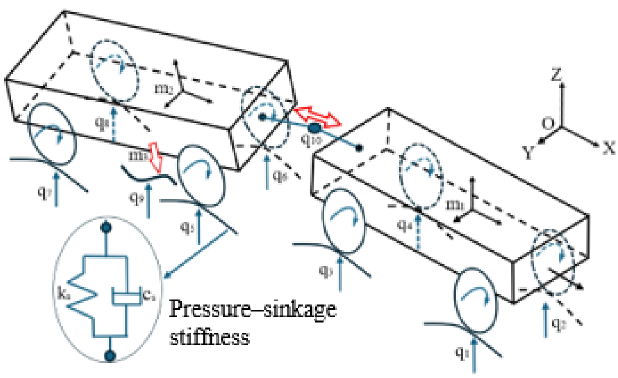

Fig. 2: Dynamic model of the coupled tractor-working machine-shallot planting head system
Source: created by the authors

The selected 8-DOF model captures the dominant vertical and rotational motions relevant to shallot planting under low-speed field conditions, including coupling-induced yaw and planting head-soil interaction. Higher-order flexibilities are not considered to maintain computational efficiency for system-level vibration assessment. If the formulation were reduced by neglecting the coupling yaw motion or the vertical dynamics of the planting head, the model would no longer capture transient load transfer and peak responses induced by pulse-type terrain excitations. Such simplifications may underestimate critical dynamic loads acting on the planting unit under irregular field conditions, which is a key motivation for retaining the selected degrees of freedom.

Based on the modeling assumptions described and the parameters in Table 1, the dynamic behavior of the shallot planter union is formulated using the Euler–Lagrange approach. The generalized coordinate vector of the system is defined as

$$\mathbf{q} = [z_1\ \phi_1\ \theta_1\ z_2\ \phi_2\ \theta_2\ z_t\ \psi_3]^{T},$$

The generalized coordinates include the tractor vertical displacement and pitch/roll (z_1, ϕ_1, θ_1), the working machine vertical displacement and pitch/roll (z_2, ϕ_2, θ_2), the planting head vertical displacement (z_t), and the coupling yaw rotation (ψ_3). All generalized coordinates are defined with respect to small perturbations about the static equilibrium configuration.

Table 1. Physical and inertial parameters of the tractor–implement system

Symbol	Description	Value	Unit
m_1	Equivalent mass of tractor	1370	kg
m_2	Equivalent mass of working machine	320	kg
m_t	Mass of shallot planting head	13.4	kg
I_{x1}	Tractor pitch moment of inertia	559.12	kg·m²
I_{y1}	Tractor roll moment of inertia	1209.85	kg·m²
I_{x2}	Working machine pitch inertia	68.68	kg·m²
I_{y2}	Working machine roll inertia	98.54	kg·m²
I_{z3}	Coupling yaw moment of inertia	10.37	kg·m²
h_1	Height of tractor CG	0.9	m
h_2	Height of working machine CG	0.6	m
l_1	Tractor axle–CG distance	0.85	m
l_2	Working machine axle–CG distance	0.6	m

The physical and inertial parameters reported in Table 1 are treated as nominal values and were obtained from manufacturer specifications, technical documentation, and commonly adopted parameter sets reported for tractor–implement systems of comparable size and configuration. Although explicit measurement uncertainty is not listed for each parameter, the reliability of the conclusions is supported through response-based sensitivity interpretation using RMS and peak metrics in Section 3, which indicates how variations in stiffness, damping, and soil properties affect vibration transmission to the planting unit.

2.2 Euler–Lagrange Formulation

2.2.1 General Equations

The equations of motion are derived using the Euler–Lagrange method with the Lagrangian defined by (1)

$$L = T - V \tag{1}$$

where T denotes the kinetic energy and V represents the potential energy of the system.

The kinetic energy includes the translational and rotational contributions of the tractor, the working machine, and the shallot planting head. Although the translational inertia of the coupling joint is neglected due to its relatively small mass, its yaw rotational inertia is retained to capture coupling-induced oscillatory effects. Accordingly, the total kinetic energy of the coupled system is expressed as Eq. (2).

$$\begin{aligned} T = {} & \frac{1}{2}m_1\dot{z}_1^2 + \frac{1}{2}I_{x1}\dot{\phi}_1^2 + \frac{1}{2}I_{y1}\dot{\theta}_1^2 \\ & + \frac{1}{2}m_2\dot{z}_2^2 + \frac{1}{2}I_{x2}\dot{\phi}_2^2 + \frac{1}{2}I_{y2}\dot{\theta}_2^2 \\ & + \frac{1}{2}m_t\dot{z}_t^2 + \frac{1}{2}I_{z3}\dot{\psi}_3^2. \end{aligned} \tag{2}$$

The potential energy consists of gravitational and elastic components. Accordingly, the potential energy of the system can be expressed in the general form given in Eq. (3).

$$V = V_g + V_e, \tag{3}$$

The gravitational potential energy is given by:

$$V_g = m_1 g z_1 + m_2 g z_2 + m_t g z_t.$$

while the elastic potential energy accounts for tire–ground compliance, coupling elasticity, structural link flexibility, and soil deformation at the planting head. It is expressed as:

$$\begin{aligned} V_e = {} & \frac{1}{2}\sum_{k\in w} k_{w,k}\,\delta_{w,k}^2 + \frac{1}{2}k_{cz}\delta_{cz}^2 + \\ & \frac{1}{2}k_{cp}\delta_{cp}^2 + \frac{1}{2}k_{cr}\delta_{cr}^2 + \frac{1}{2}k_{cy}\delta_{cy}^2 + \\ & \frac{1}{2}k_{link}\delta_{link}^2 + \frac{1}{2}k_{soil}\delta_{soil}^2. \end{aligned}$$

Here $\delta_{w,k}$ denotes the vertical deformation of the k-th wheel relative to the terrain profile $q_k(t)$, and $k_{w,k}$ represents the corresponding effective wheel-soil vertical stiffness. The excitation input $q_9(t)$ describes the vertical displacement of the soil surface beneath the planting head. In the present model, the key deformations are defined as:

$$\delta_{cz} = z_1 - z_2, \delta_{cp} = \phi_1 - \phi_2, \delta_{cr} = \theta_1 - \theta_2$$
$$\delta_{cy} = \psi_3, \delta_{link} = z_t - z_2, \delta_{soil} = z_t - q_9(t)$$

Tractor wheel: $\delta_{w,k} = z_{1,k} - q_k(t)$,
with $z_{1,k} = z_1 \pm a_1\phi_1 \pm \frac{w_1}{2}\theta_1, k = 1\ldots4$

Working machine wheel: $\delta_{w,k} = z_{2,k} - q_k(t)$,
with $z_{2,k} = z_2 \pm a_2\phi_2 \pm \frac{w_2}{2}\theta_2, k = 5\ldots8$

The signs depend on font/real, left/right wheel locations.

To incorporate viscous damping effects in a consistent manner, a Rayleigh dissipation function is introduced as

$$\mathcal{D} = \frac{1}{2}\dot{q}^T C\dot{q}.$$

where C is the system damping matrix includes contributions from suspension damping, coupling damping, and soil-related energy dissipation.

The Euler–Lagrange equation to each general coordinate of q_i according to the equation (4)

$$\frac{d}{dt}\left(\frac{\partial L}{\partial \dot{q}_i}\right) - \frac{\partial L}{\partial q_i} + \frac{\partial \mathcal{D}}{\partial \dot{q}_i} = Q_i \quad (4)$$

After linearization about the static equilibrium configuration, the kinetic and potential energies can be written as:

$$T = \frac{1}{2}\dot{q}^T M\dot{q},\ V = \frac{1}{2}q^T Kq.$$

Accordingly, the matrix entries are obtained as:

$$M_{i,j} = \frac{\partial^2 T}{\partial \dot{q}_i \partial \dot{q}_j}, C_{i,j} = \frac{\partial^2 \mathrm{D}}{\partial \dot{q}_i \partial \dot{q}_j}, K_{i,j} = \frac{\partial^2 V}{\partial q_i \partial q_j}.$$

The equations of motion can be expressed in the standard matrix form given in Eq. (5).

$$M\ddot{q} + C\dot{q} + Kq = Q_{exc}(t). \quad (5)$$

where M, C, and K denote the mass, damping, and stiffness matrices of the system, respectively. The excitation vector $Q_{exc}(t)$ collects terrain-induced base excitations, coupling interactions, and soil reaction forces acting on the planting head.

Accordingly, the oscillatory dynamics of the coupled system with eight degrees of freedom can be described by the system of differential equations given in Eq. (6), the coupling interaction is introduced only in the equations governing the tractor, the working machine, and the relative yaw motion at the joint. The coupling is modeled as a linear elastic-damping element acting on the relative vertical and rotational motions between the tractor and the working machine. Accordingly, the vertical coupling forces $F_{coupling,1}$ and $F_{coupling,2}$ as well as the associated coupling moments $M_{coupling,x}$ and $M_{coupling,y}$, represent internal interaction forces transmitted through the joint and appear only in the corresponding equations of these subsystems. The yaw degree of freedom ψ_3 is governed by the rotational stiffness and damping of the coupling joint, which generates a restoring moment proportional to ψ_3 and its time derivative.

$$F_{coupling,1} = -k_{c,z}(z_2 - z_1) - c_{c,z}(\dot{z}_2 - \dot{z}_1)$$
$$F_{coupling,2} = +k_{c,z}(z_2 - z_1) + c_{c,z}(\dot{z}_2 - \dot{z}_1)$$

while the yaw coupling moment is given by

$$M_{coupling,\psi} = k_{c,\psi}\psi_3 + c_{c,\psi}\dot{\psi}_3$$

In contrast, the vertical dynamics of the shallot planting head are not directly affected by the coupling forces but are governed by the soil–tool interaction, including soil stiffness, soil damping, and terrain-induced excitation, as reflected in the last equation of Eq. (6).

$$\begin{aligned}
&m_1\ddot{z}_1 + c_1\dot{z}_1 + k_1 z_1 = F_1(t) + F_{coupling,1} \\
&I_{x1}\ddot{\phi}_1 + c_{\phi1}\dot{\phi}_1 + k_{\phi1}\phi_1 = M_{x1}(t) + M_{coupling,x1} \\
&I_{y1}\ddot{\theta}_1 + c_{\theta1}\dot{\theta}_1 + k_{\theta1}\theta_1 = M_{y1}(t) + M_{coupling,y1} \\
&m_2\ddot{z}_2 + c_2\dot{z}_2 + k_2 z_2 = F_2(t) + F_{coupling,2} \\
&I_{x2}\ddot{\phi}_2 + c_{\phi2}\dot{\phi}_2 + k_{\phi2}\phi_2 = M_{x2}(t) + M_{coupling,x2} \\
&I_{y2}\ddot{\theta}_2 + c_{\theta2}\dot{\theta}_2 + k_{\theta2}\theta_2 = M_{y2}(t) + M_{coupling,y2} \\
&I_{z3}\ddot{\psi}_3 + c_{\psi3}\dot{\psi}_3 + k_{\psi3}\psi_3 = M_{z3}(t) \\
&m_t\ddot{z}_t + (c_t + c_{soil})\dot{z}_t + (k_t + k_{soil})z_t \\
&\qquad = c_{soil}\dot{q}_9(t) + k_{soil}q_9(t)
\end{aligned} \quad (6)$$

It is noted that the coupling forces satisfy action-reaction pairs and do not introduce additional external work into the overall system.

2.2.2 Soil Stimulation and Interaction Models

To close the dynamic model defined in Eq. (2.6), the external excitation sources and interaction forces acting on the system are specified as follows. Excitation from the field surface is represented using harmonic (sinusoidal) terrain profiles. Soil settlement and the corresponding soil reaction forces are evaluated based on the Bekker pressure–sinkage model and subsequently linearized within the operating range to facilitate state-space formulation and oscillation analysis.

Accordingly, the field-induced excitation inputs $q_1, q_2, \dots, q_{10}$ are modeled as sinusoidal functions, as expressed by Eq. (7).

$$q_i(t) = A_i \sin(\omega_i t + \phi_i) \tag{7}$$

The excitation amplitudes were selected to represent typical terrain irregularities encountered during shallot planting operations on soft and uneven fields, rather than extreme or failure conditions. The adopted harmonic components are intended to approximate realistic surface profiles consistent with low-speed agricultural operation scenarios. Moreover, the excitation frequency can be related to the tractor forward speed v and a characteristic terrain wavelength λ via $f \approx v/\lambda$. This relation provides a physical interpretation of the dominant frequency range observed in the simulations (approximately 0.5–2 Hz) and supports the relevance of the frequency-domain results to practical operating conditions.

Bekker provides pressure-sinkage $P(z)$. The soil reaction force is obtained $F_{soil} = P.A$ as linearized about z_0 as expressed by Eq. (8).

$$F_{soil} \approx F_0 + c_{soil}\dot{z}_t + k_{soil}(z_t - z_0) \tag{8}$$

The coupling forces between the tractor and the working machine are modeled as linear elastic-damping elements acting on the relative translational and rotational motions at the joint. This formulation captures the dominant energy transfer mechanism through coupling while avoiding unnecessary model complexity.

2.2.3 State-Space Models

The second-order differential equation system given in Eq. (6) is transformed into an equivalent state-space representation, as expressed in Eq. (9). The resulting state vector consists of 16 state variables, representing the generalized displacements and velocities of the system degrees of freedom.

The corresponding state-space matrices A, B, C, and D are constructed according to the system parameters and are summarized in Table 2. These matrices are subsequently implemented in the Matlab/Simulink environment for numerical simulation and dynamic response analysis.

$$\begin{aligned} \dot{x} &= Ax + Bu \\ y &= Cx + Du \end{aligned} \tag{9}$$

Table 2. Status matrices

Matrix	Dimensions	Meaning
A	16×16	system state dynamics
B	16×10	input excitation distribution
C	16×16	output selection/observation
D	16×10	direct feedthrough

Source: created by the authors

The x(t) state vector consists of 16 components that describe the position and velocity of 8 degrees of freedom:

$$x(t) = [z_1, \phi_1, \theta_1, z_2, \phi_2, \theta_2, z_t, \psi_3, \dot{z}_1, \dot{\phi}_1, \dot{\theta}_1, \dot{z}_2, \dot{\phi}_2, \dot{\theta}_2, \dot{z}_t, \dot{\psi}_3]^T$$

The input vector u(t) consists of 10 excitation force signals from the field surface:

$$u(t) = [q_1(t), q_2(t), q_3(t), q_4(t), q_5(t), q_6(t), q_7(t), q_8(t), q_9(t), q_{10}(t)]^T$$

State-space representation provides a convenient framework for future control-oriented studies. While observability and controllability analyses are beyond the scope of the present work, the selected state variables represent physically meaningful quantities and form a suitable basis for subsequent controller design and vibration mitigation research.

3 Problem Solution

3.1 Matlab/Simulink Simulation

The overall structure of the Simulink model consists of several functional blocks. The Input Excitation block includes ten excitation signals, where $q_1 \div q_8$ represent the ground-induced excitation forces acting on the wheels, q_9 denotes the excitation force applied to the shallot planting head, and q_{10} corresponds to the excitation force acting on the coupling joint.

The system dynamics are implemented in the State-Space block, which is defined by the standard state-space representation:

$$\dot{x} = Ax + Bu, \ y = Cx + Du$$

where x is the state vector and u is the input excitation vector.

The Signal Processing block employs demultiplexing operations to separate the state variables and compute the corresponding displacement, velocity, and acceleration responses. Finally, the Signal Visualization block uses scope and plot modules to observe and analyze the system responses. A schematic diagram of the overall Simulink model structure is presented in Figure 3.

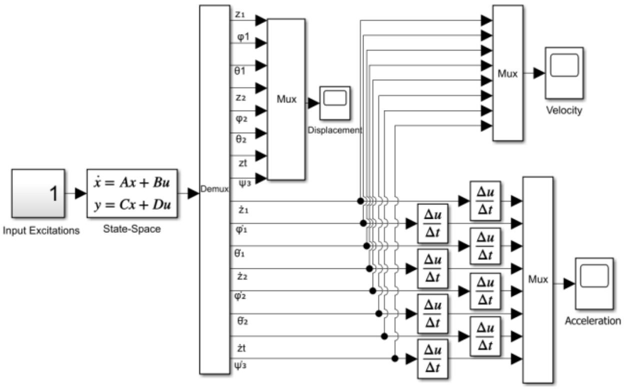

Fig. 3: Simulink block diagram of the state-space model
Source: created by the authors

3.2 Simulation and Discussion Results

3.2.1 LHM Simulation Results

The stability of the tractor–implement–planting head system was evaluated using the eigenvalues of the state matrix A. As shown in Figure 4(a), all eigenvalues are in the left half of the complex plane, with the maximum real part maxR(λ)=−2.8782, confirming that the system is asymptotically stable.

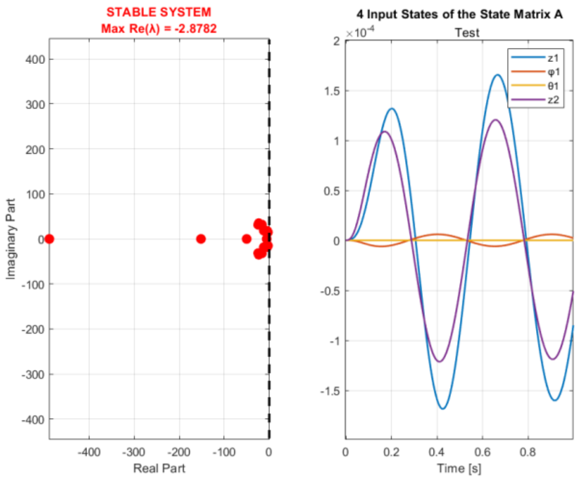

(a) (b)

Fig. 4: Survey graph affecting parameters associated with system stability
Source: created by the authors

The responses under four initial state perturbations Figure 4(b) remain bounded and converge to steady oscillations without drifting or amplification, with response magnitudes on the order of 10^{-4}. This behavior provides a consistency check for the developed state-space implementation.

Three representative road roughness excitations were applied at the tractor wheels (Figure 5), including harmonic, random, and pulse-type inputs. The harmonic excitation produces a steady periodic input, the random excitation results in broadband fluctuations, and the pulse-type excitation generates short-duration impulses representing the most severe condition in terms of peak disturbance levels.

Fig. 5: The input stimuli act on the wheels of the tractor
Source: created by the authors

Figure 6 shows the tractor responses in vertical displacement z_1, pitch angle ϕ_1, and roll angle θ_1. The responses remain stable under all excitation types. Pulse-type excitation yields pronounced transient peaks compared with harmonic and random cases, indicating that the tractor response is mainly governed by impulsive disturbances. For rotational motions, the pitch response is consistently more pronounced than the roll response, implying that longitudinal oscillations dominate the tractor dynamics.

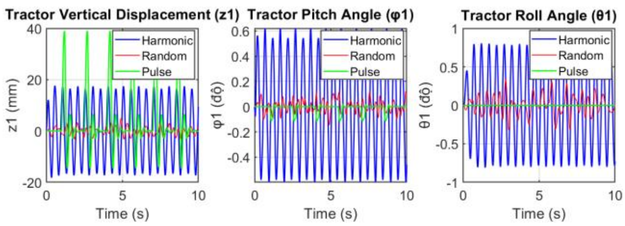

Fig. 6: Dynamic response of tractor vertical displacement
Source: created by the authors

The working machine responses are presented in Figure 7. Compared with the tractor, the working machine exhibits stronger sensitivity to terrain-induced disturbances, particularly under pulse excitation, where the vertical displacement z_2 shows larger transient peaks. The rotational responses ϕ_2 and θ_2 remain bounded but reveal higher fluctuation levels, consistent with the effect of elastic coupling between the two subsystems.

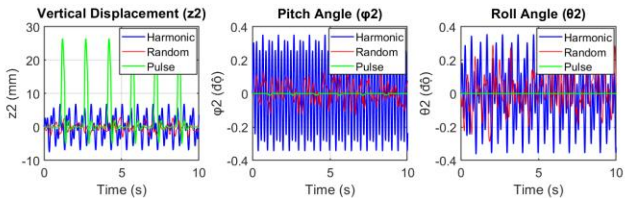

Fig. 7: Dynamic response of working machine vertical displacement
Source: created by the authors

Figure 8 reports the responses of the shallot planting head displacement z_t and the coupling yaw angle ψ_3. The planting head shows limited vibration levels under harmonic and random excitations, whereas pulse excitation produces distinct displacement spikes, which may affect planting depth consistency. The coupling yaw angle exhibits the largest transient peaks under pulse excitation, indicating that the coupling joint is a critical location for vibration transmission within the coupled system.

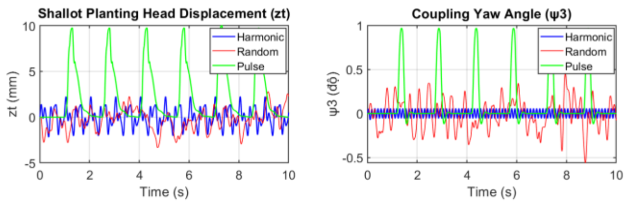

Fig. 8: Vertical displacement of the planting head and yaw angle of the coupling joint
Source: created by the authors

A quantitative comparison of RMS and maximum responses is provided on Figure 9. The RMS values reflect sustained vibration levels associated with operational smoothness, whereas the maximum responses under pulse excitation capture extreme transient loads relevant to durability assessment. The comparison highlights z_t, ψ_3, and ϕ_2 as critical response states, under severe disturbances.

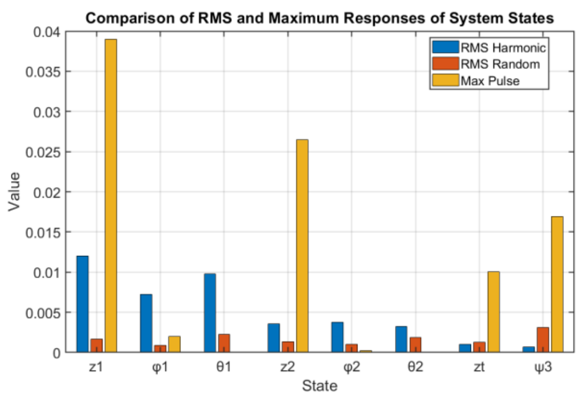

Fig. 9: Stability test graph and RMS analysis
Source: created by the authors

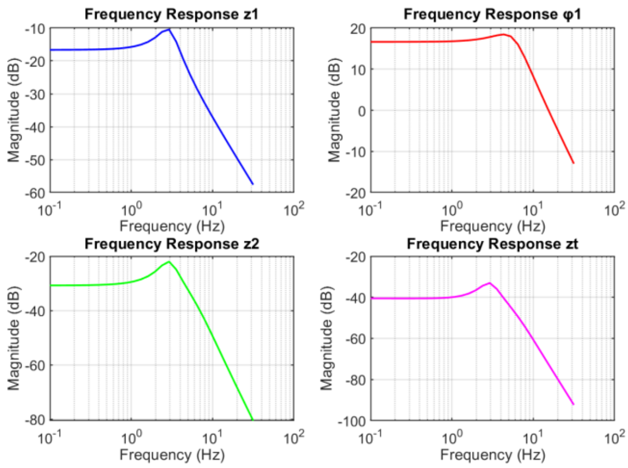

Fig. 10: Frequency response of the coupled system states
Source: created by the authors

The frequency-domain results Figure 10 indicate that the dominant resonances of the vertical motions z_1 and z_2 occur in the low-frequency range of approximately 0.5–2 Hz, which is characteristic of body-mode dynamics in low-speed vehicle-implement systems. The planting head response remains lower in magnitude than the main-body vertical motions across the analyzed band, suggesting that the most critical planting head excursions are primarily associated with transient pulse-type inputs.

3.2.2 Discuss the Results

The dynamic responses obtained in the present study are consistent with trends reported in recent investigations of agricultural vehicle and multibody system dynamics. Low-frequency vibration components dominate the system response, which aligns with tractor dynamics simulations conducted under realistic operating conditions, [4], [5]. Such low-frequency behavior is commonly associated with vehicle body modes and coupling dynamics, indicating that suspension stiffness, damping, and joint compliance play a critical role in vibration transmission.

The sensitivity of the simulated responses to soil stiffness and damping parameters is in agreement with soil–vehicle interaction studies reported in the literature. [3] demonstrated that variations in soil stiffness constants significantly influence the dynamic behavior of agricultural machinery operating on paddy soils. Similarly, investigations incorporating deformable terrain models have shown that soil compliance and contact modeling assumptions can amplify transient loads and alter resonance characteristics if not adequately represented, [7]. The present results confirm that soil–tool interaction must be explicitly considered when evaluating vibration behavior of planting units, [8].

The influence of coupling dynamics observed in this study is also consistent with multibody modeling results reported for articulated and tractor–trailer systems. [5] and [10] showed that coupling geometry and joint dynamics strongly affect system stability and transient response. In the present model, the inclusion of yaw dynamics at the coupling joint provides additional insight into internal force transmission mechanisms that are not captured in tractor-only formulations. Similar stability considerations have been reported for coupled vehicle systems operating under demanding conditions, [11].

From a methodological standpoint, the state-space representation employed in this work enables a systematic stability analysis of the coupled system. State-space and multibody formulations have been widely adopted to analyze the dynamic behavior of mechanical systems with multiple degrees of freedom, [13]. Within the WSEAS framework, earlier conference contributions demonstrated the applicability of state-space-based dynamic modeling to vibration and stability analysis in complex mechanical systems, [9]. The marginal-to-stable behavior identified in the eigenvalue analysis of the present study highlights the importance of damping and parameter tuning, which is consistent with general stability principles reported in recent vehicle and multibody dynamics literature, [11].

4 Conclusion

A coupled dynamic model of shallot planter union was developed and implemented in a MATLAB/Simulink environment to investigate vibration behavior under soft-soil operating conditions. The model integrates tractor and working machine dynamics with elastic coupling effects and a Bekker-based soil interaction description, allowing the main vibration transmission mechanisms within the system to be examined.

The simulation results confirm asymptotic stability of the coupled system and show that transient terrain disturbances play a dominant role in generating peak dynamic responses. Coupling yaw motion and planting head displacement were identified as critical response states, while frequency-domain analysis revealed low-frequency amplification associated with body-mode dynamics of the tractor–implement assembly. These findings are consistent with trends reported in multibody and soil-machine interaction studies.

The proposed modeling framework provides a physically interpretable and computationally efficient tool for preliminary vibration assessment and parameter tuning of shallot planting machinery. Future work will focus on field experiments for parameter calibration, extension to spatially varying soil properties, and the exploration of vibration mitigation strategies aimed at improving planting stability and uniformity.

Acknowledgement:
The authors would like to express their sincere gratitude to Vinh Long University of Technology Education for providing support and favorable conditions for this study.

References:

[1] Y. Yu, Y. joo Kim, and N. Noguchi, "A non-linear dynamic model for agricultural vehicles constructed in digital space," *Smart Agricultural Technology*, vol. 11, Aug. 2025, doi: 10.1016/j.atech.2025.100891.

[2] M. G. Bekker, Introduction to Terrain–Vehicle Systems, University of Michigan Press, Ann Arbor, MI, USA, 1969. ISBN: 978-0472041442.

[3] Q. Jiang, M. Cao, Y. Wang, J. Wang, and Z. He, "Quantification of the soil stiffness constants using physical properties of paddy soils in Yangtze Delta Plain, China," *Biosyst. Eng.*, vol. 200, pp. 89–100, Dec. 2020, doi: 10.1016/j.biosystemseng.2020.09.004.

[4] X. Zhao, Y. Du, E. Mao, Z. Zhu, and Z. Song, "Agricultural tractor dynamics simulation research based on a driving simulator with real-time human-machine interaction," *Comput. Electron. Agric.*, vol. 203, Dec. 2022, doi: 10.1016/j.compag.2022.107443.

[5] B. Zhou, S. Chen, J. Hu, Y. You, D. Wang, and Q. Zhang, "Multi-body dynamics modeling and test of an articulated steering half-track tractor," *International Journal of Agricultural and Biological Engineering*, vol. 16, no. 6, pp. 124–133, 2023, doi: 10.25165/j.ijabe.20231606.8165.

[6] M. A. Son *et al.*, "Development and performance evaluation of lateral control simulation-based multi-body dynamics model for autonomous agricultural tractor," *Korean Journal of Agricultural Science*, vol.

50, no. 4, pp. 773–784, Dec. 2023, doi: 10.7744/kjoas.500415.

[7] K. Aoshima and M. Servin, "Examining the simulation-to-reality gap of a wheel loader digging in deformable terrain," *Multibody Syst. Dyn.*, vol. 64, no. 1, pp. 121–148, May 2025, doi: 10.1007/s11044-024-10005-5.

[8] W. Liu, S. Zeng, and X. Chen, "Design and Experiment of Adaptive Profiling Header Based on Multi-Body Dynamics–Discrete Element Method Coupling," *Agriculture (Switzerland)*, vol. 14, no. 1, Jan. 2024, doi: 10.3390/agriculture14010105.

[9] C. Alexandru and P. Alexandru, "Dynamic Modeling and Simulation in Virtual Environment of an Active Suspension System," in *Proceedings of the WSEAS International Conference on Systems*, Corfu, Greece, 2010, [Online]. https://www.wseas.us/e-library/conferences/2010/Corfu/SYSTEMS/SYSTEMS1-09.pdf (Accessed Date: January 10, 2026).

[10] M. Moll and T. Oksanen, "Kinematic and Dynamic Modeling of a Generalized Tractor-Trailer System with Steering Actuation," in *IFAC-PapersOnLine*, Elsevier B.V., Feb. 2025, pp. 199–204. doi: 10.1016/j.ifacol.2025.03.035.

[11] H. Cai and X. Xu, "Lateral Stability Control of a Tractor-Semitrailer at High Speed," *Machines*, vol. 10, no. 8, Aug. 2022, doi: 10.3390/machines10080716.

[12] H. Wang and N. Noguchi, "Real-time states estimation of a farm tractor using dynamic mode decomposition," *GPS Solutions*, vol. 25, no. 1, Jan. 2021, doi: 10.1007/s10291-020-01051-5.

[13] C. M. Pappalardo, "Dynamic Analysis of Multibody Mechanical Systems," Sep. 01, 2024, *Multidisciplinary Digital Publishing Institute (MDPI).* doi: 10.3390/machines12090626.

Contribution of Individual Authors to the Creation of a Scientific Article (Ghostwriting Policy)

All authors equally contributed to the modeling, simulation, analysis, and manuscript preparation of this study.

Sources of Funding for Research Presented in a Scientific Article or Scientific Article Itself

No funding was received for conducting this study.

Conflict of Interest

The author has no conflicts of interest to declare that are relevant to the content of this article.